IOP Publishing Plasma Physics and Controlled Fusion
Plasma Phys. Control. Fusion **66** (2024) 125018 (10pp) https://doi.org/10.1088/1361-6587/ad8fd2

Simultaneous studies of K- and L-shell mid-atomic-number plasmas produced by Z-pinches

A Stafford*, A S Safronova, V L Kantsyrev and V V Shlyaptseva

University of Nevada, Reno, NV 89557, United States of America

E-mail: austins@unr.edu

Received 27 August 2024, revised 28 October 2024
Accepted for publication 7 November 2024
Published 21 November 2024

Abstract

Z-pinches have been intensively studied for their applications to high energy density (HED) physics, x-ray sources, astrophysics, and inertial confinement fusion. Alumel (mostly Ni) double planar wire array (DPWA) Z-pinch experiments were performed on the Zebra generator at the enhanced current of 1.6 MA with an advanced setup of diagnostics to measure the temporal evolution of x-ray radiation from plasmas. The implementation of two time-gated spectrometers which recorded hard and soft x-ray radiation allowed for simultaneous studies of K-shell and L-shell radiating plasmas, respectively, in a single experiment. Two almost identical DPWA experiments established a wide observation window around the main x-ray burst. Overall, time-gated plasma spectroscopy provided more information on temporal evolution of 'hot' and 'cold' K-shell radiating plasmas compared to slowly evolving L-shell radiating plasma. In addition, new spectral features such as from hollow ions were observed and studied using the time-gated K-shell plasma spectroscopy, which is important for further investigation of exotic ion states in HED plasmas.

Keywords: Z-pinch, x-ray diagnostics, plasma spectrsocopy, time-gated K-shell Ni spectra, time-gated L-shell Ni spectra, hollow Ni ions

1. Introduction

Z-pinches have been studied for their applications to high energy density (HED) physics [1–3], astrophysics [4–6], and inertial confinement fusion [7, 8]. Particular aspects of interest include electron beam formation [9, 10] and plasma jet formation using wire arrays [11]. Electron beam formation is of interest as it can create excited ion states when interacting with colder plasma that can lead to characteristic radiation such as 'cold' Kα and, if the electron beam is anisotropic, polarized emission. Plasma jet interactions play a role in inertial confinement fusion and understanding them is important for optimizing the implosion dynamics on the target material. Planar wire arrays have been found to be particularly efficient Z-pinch x-ray radiators [11–13]. A comprehensive overview of Z-pinches can be found in Haines 2011 [1].

K-shell radiation from Z-pinches for many materials (Al, Cu, Ni, Fe, etc.) has been studied on large scale machines such as Z (>15 MA) [14] at Sandia National Laboratories and smaller scale machines such as Zebra (~1 MA) [9, 11–13, 15] at the University of Nevada, Reno. The research corroborated theoretical predictions of the necessary electron temperatures (T_e) needed to produce significant K-shell radiation for a material as determined by the Naval Research Laboratory [16, 17]. The predicted $T_e = 0.3^*Z^{2.9}$ eV was matched up to Cu for experiments on the Z machine, whereas Ti was the limit for the Zebra machine. Similar studies were conducted on Zebra for L-shell radiators [18]. Mid-atomic-number materials including stainless steel, Alumel, Cu, brass, Mo, and Ag were considered with the highest electron temperatures observed from L-shell radiation coming from Ag wire pinches.

* Author to whom any correspondence should be addressed.

The ionization balance is connected to many important aspects of understanding plasma [19]. The degree of ionization is connected to the total energy in the system. Each additional electron excited away from an ion tends to take an increased amount of energy with much larger increases when breaking into a new shell. Therefore an accurate understanding of the ionization balance can help to determine the energy accumulated in the plasma. The ions in the system produce line emission that varies with the ionization stages present. The radiated energy leaving the system plays a part in the cooling of the system. Understanding this radiation loss is important for predicting plasma evolution in time. Along with radiation emission, the different ions absorb radiation differently. An accurate ionization balance improves considerations of the radiation transport effects in the system, whether by external sources passing through or from the internal emission being reabsorbed. Many important diagnostic tools for analyzing plasma are spectroscopic in nature. These tools are unintrusive when working with the radiation naturally produced by the plasma. Modeling the observed spectra produced by the plasma can provide insight into many plasma conditions including temperature and density. For the models to be able to accurately match the emitted spectra, they need to be able to estimate the ionization balance with sufficient precision. Multiple workshops have been dedicated to the improvement of non-Local Thermodynamic Equilibrium (non-LTE) modeling with the prediction of ionization balance as a point of emphasis [20–23]. However, time integrated spectroscopy or studies of one particular type of plasma (such as K-shell or L-shell radiating plasma) frequently are not able to provide sufficient information about HED plasmas. We are aware of only a few studies where the various types of radiation from different ionization stages from both the K-shell and L-shell radiating plasmas were measured simultaneously, such as the one that was done by Ouart *et al* [20, 24] for ultrashort laser produced Fe plasma. The simultaneous K-shell and L-shell radiation was used to highlight the differences between the laser prepulse contrasts and main pulse durations. For example, a comparison of the intensity of the Kα and Ne-like 3D ($1s^2 2s^2 2p^2{}_{1/2} 2p^3{}_{3/2} 3d_{5/2}$ $J = 1 \rightarrow 1s^2 2s^2 2p^6$ $J = 0$) lines decreased as the prepulse increased. This is why here we are presenting the results of experimental and theoretical work based on time-resolved monitoring and time-gated spectroscopy of Z-pinch plasmas.

This paper highlights the results of experiments with double planar wire arrays (DPWA) from Alumel wires. Alumel has been studied in detail as part of a search for efficient x-ray radiators for mid-atomic-number materials [11]. Time-gated recordings of both K-shell and L-shell Ni radiation are analyzed through identifying the ionization stages that are present and by comparing to theoretical modeling to estimate plasma parameters. Radiation detecting diodes are used to determine the timing of the spectra within the implosion process.

2. Experimental details and implosion characteristics

Experiments were done on the Zebra generator at the University of Nevada, Reno. The Zebra generator is a pulsed power device that produces 1 MA currents [25] under standard operation and up to 1.7 MA when the load current multiplier (LCM) is used [26]. Load characteristics and experimental details of two Alumel (96% Ni, 2% Si, 2% Al) DPWAs are listed in table 1. The DPWAs consisted of 12 wires per plane with a 6 mm interplanar gap, 0.7 mm interwire gap, and 1 cm anode to cathode gap. The two shots were identical except for a small difference in load mass (192 vs 173 μm) which was adjusted to bring the main implosion closer to the peak current for the second shot. The primary diagnostics fielded during the experiments were x-ray detecting diodes, time-gated spectrometers, and two frames of shadowgraphy. The three x-ray detecting diodes cover three different radiation cutoffs of >0.2 keV (<62 Å) XRD, >0.7 keV (<17.7 Å) PCD, and >9 keV (<1.38 Å) SiD. The lowest energy cutoff of 0.2 keV covers the largest spectral range and is the best representation of the total radiation emitted throughout the experiment. The middle energy cutoff of 0.7 keV is a better representative of the soft L-shell Ni radiation being emitted in time. The high energy cutoff of 9 keV is the best representative of the hard K-shell Ni radiation. The two time-gated spectrometers observed different spectral regions focused on recording K-shell Ni (∼1.3–1.8 Å) using a LiF crystal (2d = 4.028 Å) (TGHXR spectrometer with 6 observation frames) and L-shell Ni (∼8–12 Å) using a KAP crystal (2d = 26.634 Å) (TGSP spectrometer with 4 frames of observation). The spectrometers utilize a micro channel plate (MCP) to acquire the spectral data at selected timings. The time-gated spectrometers are operated as spatially integrated. The limited radiation available in the short time frame makes further limitations, such as by including a slit, reduce the observable radiation too low to reliable record. Current and x-ray diode signals, as well as time-gated spectrometers timings are shown for shots 3253 and 3254 in figures 1(a) and (b), respectively. The final diagnostic was a bolometer used to determine the total radiation yield for each shot.

Shot 3253 used Alumel wires of 10.7 μm diameter for a total mass of 192 μg and it produced a total radiation yield of 10.1 kJ. The current peaks around 1.6 MA at 97 ns after the current start and the main implosion occurs at 104 ns after current start as detailed by the first major peak measured by the different diodes. Other than the XRD, all the signals have a sharp increase into the first peak which is followed by three subsequent peaks and the slower decay back to baseline which represents the main implosion with additional small implosions produced by the trailing mass. The main burst of the radiation lasts approximately 45 ns. Below the signals from

Table 1. Load characteristics and experimental details of two alumel double planar wire array (DPWA) experiments. Each plane has 12 wires with 0.7 mm interwire gap placed at the distance of 6 mm. All times are counted from the current start.

Zebra shot number	Load config.	Load geometry	Load mass (μg)	Implosion time (ns)	Current (MA)	Bolometer (kJ)	TGHXR times (ns)	TGSP times (ns)
3253	DPWA	0.7 mm/6 mm	192	104	1.58	10.1	75–100	83–98
3254	DPWA	0.7 mm/6 mm	173	98	1.62	10.4	91–116	95–110

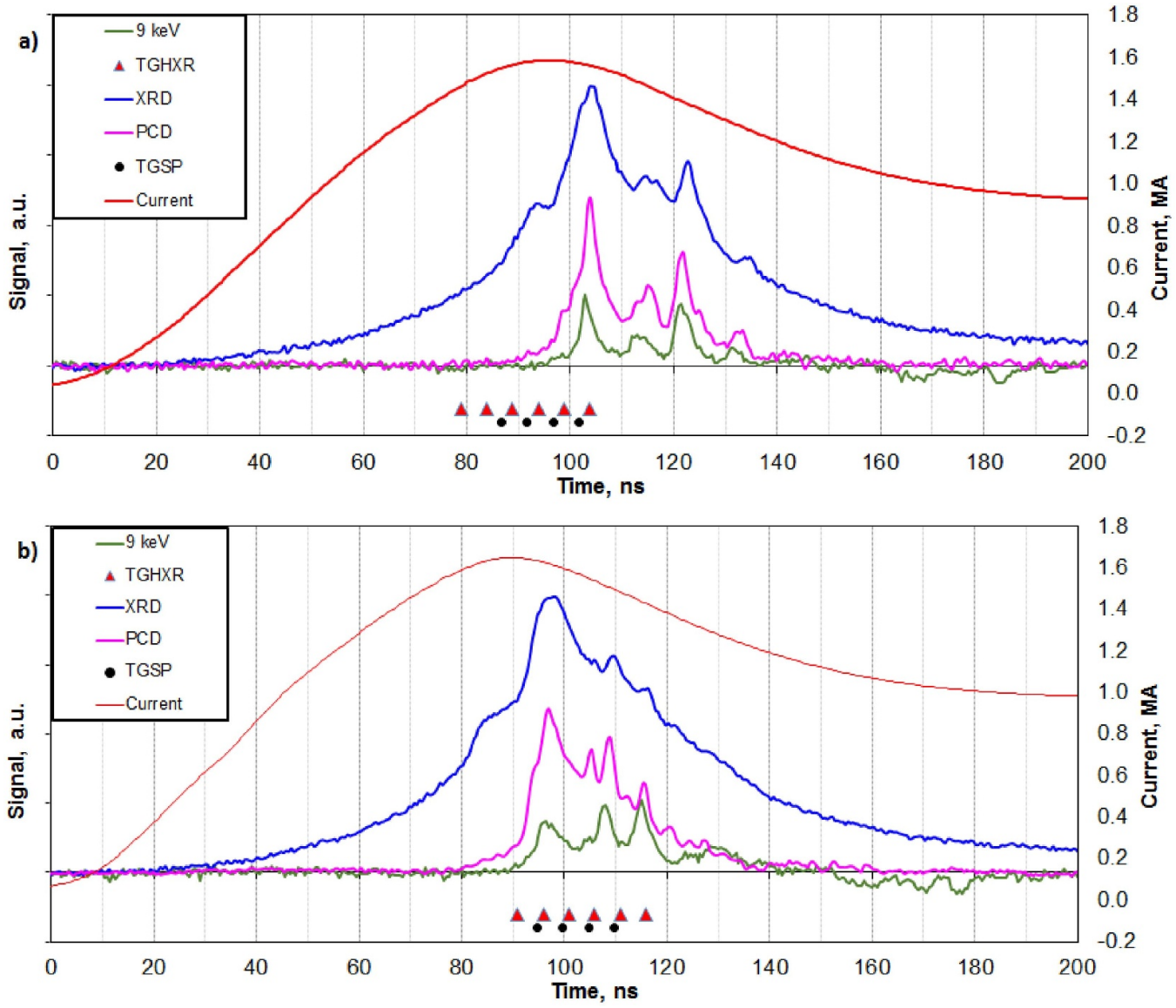

Figure 1. Alumel DPWAs produced in Zebra shots 3253 (a) and 3254 (b). Current and x-ray diode signals shown together with the timing of x-ray time-dated spectrometers (TGHXR for hard x-rays and TGSP for softer x-rays). See the text for more details.

the diodes are the markers for when the two time-gated spectrometers were triggered. The K-shell focused spectrometer is represented by the red triangles and labeled TGHXR. The timings for this shot were initiated before the start of the main implosion and continued up to its onset. The L-shell focused spectrometer is represented by the black circles, labeled TGSP, and was targeted in a similar manner to the TGHXR spectrometer although it only consisted of four frames compared to the six of the TGHXR. Timings for the two shadowgraphy frames are represented by the orange circles.

Shot 3254 used 10.16 μm diameter wires to reduce the total mass so that the main implosion would occur closer to the current peak. The total radiation yield for this shot was 10.4 kJ. The structure of the observed signals follows the same trend as shot 3253 and can be seen in figure 1(b). The notable difference is that the time-gated spectrometers were triggered later

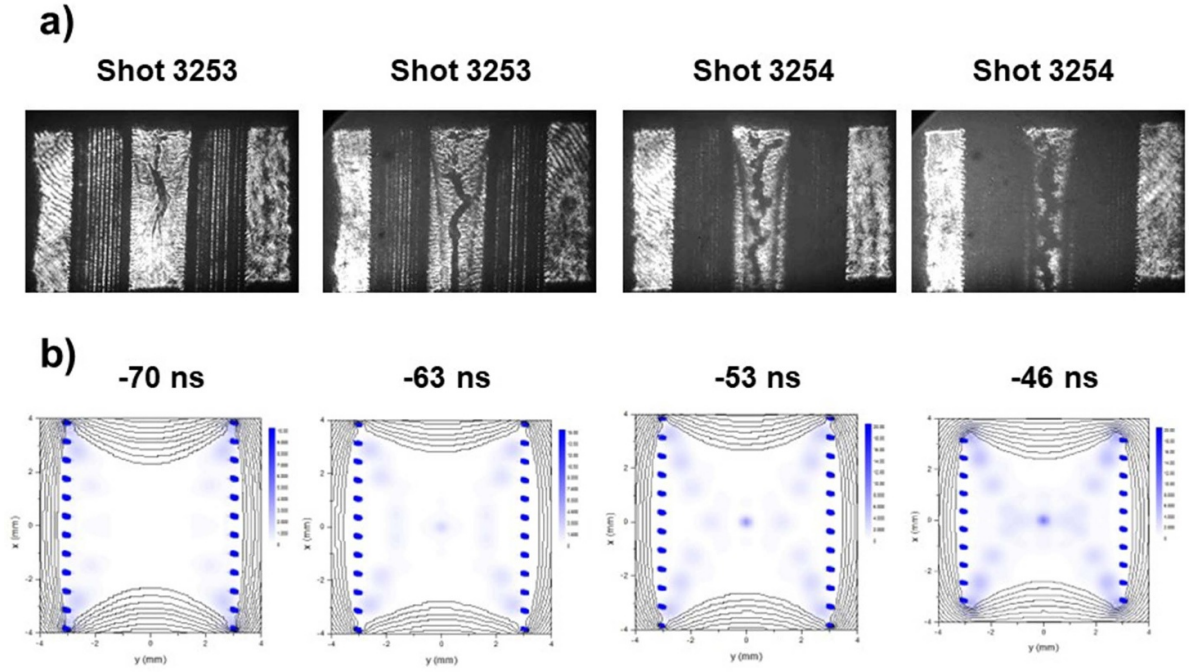

Figure 2. Shadowgraphy images of Alumel DPWAs produced in Zebra shots 3253 and 3254 (a) and end-on WADM modeling (b). Timings are relative to peak XRD power (the main x-ray burst).

into the experiment recording the beginning of the main implosion and the subsequent burst that followed. When combined with the spectra from shot 3253, a fuller look into the progression of the plasma can be seen.

Shadowgraphy diagnostic performed in these two experiments covers a period of time from −70 ns to −46 ns before the main x-ray burst. Four shadowgraphy images are displayed in figure 2(a) along with the wire ablation dynamic modeling (WADM) [27] in figure 2(b). The WADM is used to predict and compare wire array implosion timings to best optimize the load parameters to achieve wire array implosions near/at the current peak. The primary load parameter that differentiates the various regimes of implosion was found to be the aspect ratio defined here as the array width divided by interplanar gap [28]. In our case, the aspect ratio is 1.28 which is an intermediate ratio that allows the global magnetic field to penetrate into the interior of the array without disrupting the formation of the axial precursor. Indeed, the formation of the axial precursor is clearly observed in figure 2 both in experiment and modeling.

3. Hard x-ray time-gated K-shell spectroscopy

A detailed analysis into K-shell radiation from stainless steel X-pinch experiments with the Zebra generator was recently done by Childers *et al* [10]. It includes K-shell radiation for multiple mid-Z elements (Fe, Cr, and Ni) and details the differences in thermal and nonthermal K-shell radiation. Childers *et al* is a good source for a more comprehensive understanding of the intricacies of K-shell radiation for mid-atomic-number materials as will be considered in this paper.

Figure 3(Aa) highlights the K-shell Ni radiation recorded by the TGHXR spectrometer for shot 3253. The first three frames show no signs of K-shell Ni radiation. The fourth frame denotes the start of the K-shell radiation and is dominated by Kα emission from ionizations near Ne-like Ni. This time, labeled as −14 ns, refers to the time relative to the main implosion. The Kα emission signifies the presence of hot electrons exciting the inner shell of the bulk plasma beginning to build in the center of the array. As mentioned above, the radiation observed with the TGHXR spectrometer is best represented by the 9 keV signal from figure 1.

Figures 3(Ab) are lineouts for the spectra recorded in the film along with theoretical representations of the different ionization levels that are present in the spectra. The theoretical spectra are produced using atomic data from the FAC code [29] which is processed using the SUNR code [30–32]. The FAC code calculates the atomic levels and rates for such processes as radiative decay, radiative recombination, collisional excitation, collisional ionization, and dielectronic recombination and their inverses. Singly and double excited states were included for H-like to Al-like Ni. The singly excited states are included up to $n = 6$ for H-like ions, $n = 5$ for He- to Li-like ions, Ne- and Na-like ions, and $n = 4$ for Be- to F-like ions, and Mg- and Al-like ions. The doubly excited states include up to $n = 3$ for He-, Li-, Na-, Mg-, and Al-like ions, and with $n = 2$ for Be-like ions. The SUNR code takes these calculations and plasma parameters of electron temperature (Maxwellian distribution) and electron density defined by the user to calculate level populations through solving rate equations that consider all populating and depopulating processes for each state. The produced theoretical spectra are compared to the experimental spectra and the parameters are adjusted until a good

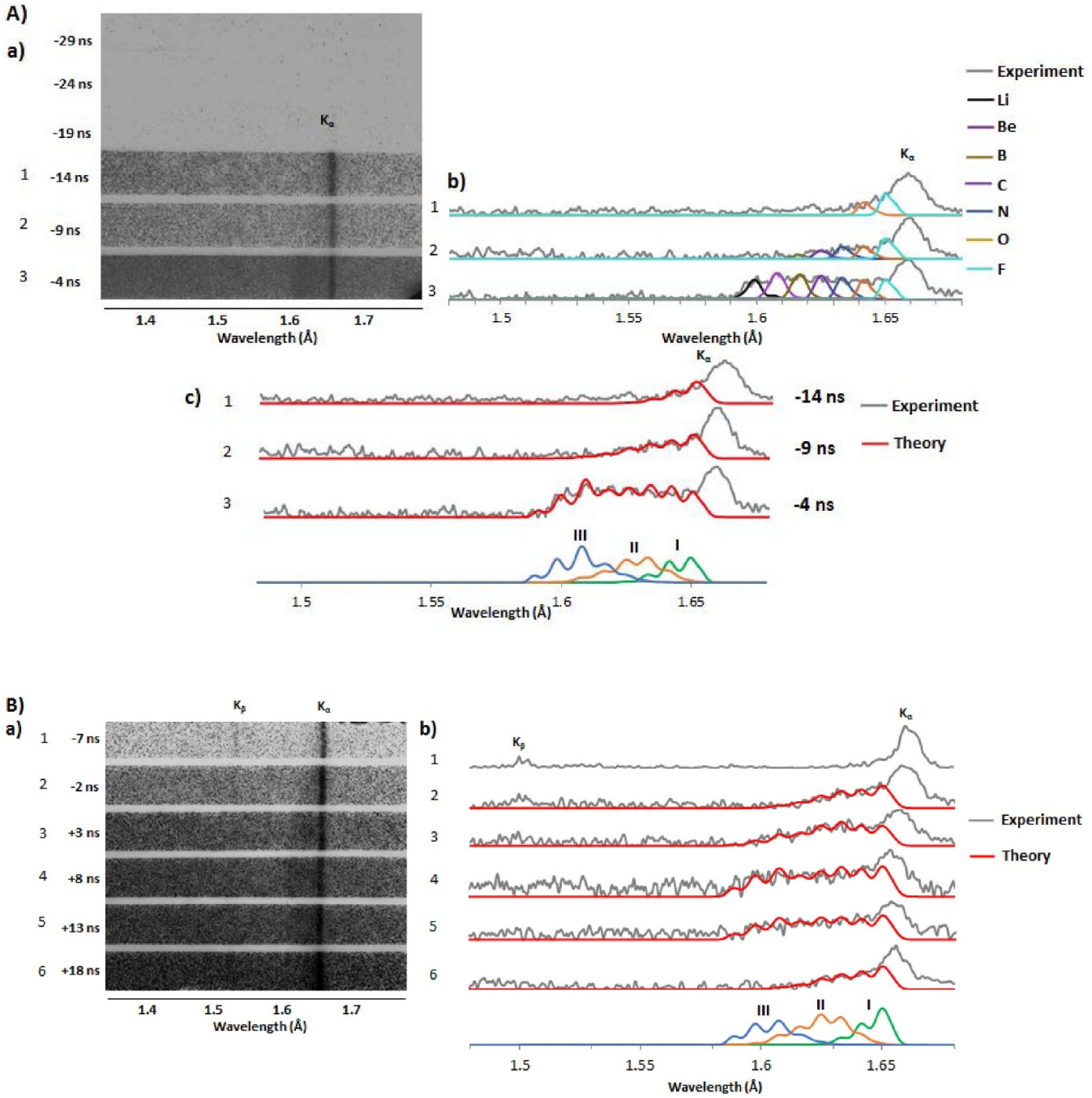

Figure 3. Hard x-ray time-gated K-shell spectra from Zebra shots 3253 (A) and 3254 (B). (Aa) and (Ba) Film from TGHXR spectrometer with timings relative to the main x-ray burst. (Ab) Lineouts from the frames shown in (Aa) fit with theoretical spectra from individual ionizations. (Ac) and (Bb) The lineouts of TGHXR spectra compared to non-LTE modeling produced from a combination of up to three spectra modeled for different values of T_e. Examples of the three individual contributions to the combined spectra used to compare with the experiment are included at the bottom with labels I, II, and III (see table 2).

fit is achieved. Plasma parameters are considered to have an error of 20% [29]. An additional parameter can be included to represent hot electrons. In this case a second electron distribution centered at a specified energy with a Gaussian distribution is added to the main Maxwellian distribution. The Gaussian distribution is weighted by an adjustable factor to represent the percentage of the electrons attributed to hot electrons. While opacity is expected to have an effect on some of the lines observed, it was not accounted for in any of the modeling as the necessary information on the physical size of the radiating source was not acquired in these experiments.

The Kα line is dominated by near Ne-like ions at this point and to the extent that the majority of the plasma will be excited under the conditions producible with the Zebra generator with the LCM for Ni. In the fifth frame at -9 ns, the left edge of the main Kα peak extends further and radiation from N-like and

C-like Ni becomes present. The sixth frame recorded at −4 ns shows a major extension of the radiation left of the main Kα peak which is found to include ionizations up to Li-like Ni when matched with the theory.

The experimental spectra from figure 3(Ab) are compared to non-LTE modeling in figure 3(Ac). This modeling focused on matching the Li-like to F-like ionizations and was composed of a combination of up to three different individually weighted electron temperatures (T_e) as the broad spread of ionizations observed in the later frames cannot be matched with a single set of plasma parameters. The large degree of overlapping of multiple ionization stages of Ne-like and lower ionization stages within the main Kα peak reduces the confidence of the wavelength calibration and therefore was not included in the modeling. Additionally, the main Kα emission from mid-atomic-number plasmas such as Ni has been shown to be affected by opacity when constituting a large percentage of the wire material [10]. The modeling of these spectra was done using a primary Maxwellian electron distribution with a secondary Gaussian electron distribution centered at 9 keV with a 50 eV HWHM and a 1% hot electron concentration. The electron density (N_e) for each frame was 5×10^{19} cm^{-3}. The first frame with K-shell spectra occurs at 14 ns prior to the main implosion and the estimated electron temperature is 100 eV. At this early timing the T_e is low relative to the typical values observed in the L-shell Ni spectra. At −9 ns a combination of two T_e (450 eV and 100 eV) is used to best match the spectra. These conditions suggest the early ablated plasma is beginning to heat up and produce localized pinches. From there, a combination of three T_e (750 eV, 450 eV, and 250 eV) is the best fit at −4 ns suggesting the hottest regions within the plasma are getting heated beyond the typical L-shell values of 300–450 eV with the main implosion soon to follow. The final lineout shows the individual contributions from the three different electron temperatures used to match the −4 ns frame, I for 250 eV, II for 450 eV, and III for 750 eV.

The six frames recorded with the TGHXR spectrometer for shot 3254 are displayed in figure 3(Ba). In the first frame, 7 ns before the main implosion, the spectra showed the main Kα peak without additional satellites, and the Kβ peak was present, unlike in shot 3253. Two nanoseconds prior to the main implosion the radiation grows to the left of the main Kα including ionizations up to B-like. This is similar to what was observed 9 ns prior to the main implosion in shot 3253. The time difference of the similar ionization levels could be due to the change in implosion time relative to the maximum current. The higher relative current in the early stages of shot 3253 could be leading to increased hot electron production relative to the amount of plasma present in the center which would increase the degree of ionization. The following frame reaches up to Li-like which is the same as the last frame from shot 3253. The fourth frame peaks at Li-like with a higher intensity than the previous frame and continues through the following frame. The last frame shows the rapid drop of the degree of ionization falling back down to C-like being the highest.

The six frames captured by the TGHXR spectrometer show a progression in the intensity of the radiation that follows the signal observed by the 9 keV diode. This is most readily seen by considering the darkening of the spectral range due to the continuum radiation. The first frame remains bright in agreement with its timing of at the very beginning of the rise in the signal of the 9 keV diode. The following five frames are much darker corresponding with the continuous intensity shown by the diode. These five frames cover the three largest peaks in the intensity. In the process of analyzing the spectra the background radiation was cut out to focus on the K-shell radiation, however, the intensity of the background adjustments were found to follow the intensity of the 9 keV signal for the coinciding time.

Figure 3(Bb) presents lineouts which were compared to non-LTE kinetic modeling composed of a combination of up to three electron temperatures as was done for shot 3253 in figure 3(Ac). All of the models for this experiment estimated the N_e at 5×10^{19} cm^{-3} and included a 1% hot electron concentration. The first frame at −7 ns was not estimated as the presence of only the main Kα and Kβ suggest Ne-like and lower ionizations which are not readily resolvable and lead to reduced confidence in the estimated T_e. The second frame at −2 ns was estimated to have a combined 100 and 450 eV T_e. The upper end of this T_e estimation is in the commonly observed range for L-shell Ni measurements and suggests the K-shell radiating plasma is likely not much hotter than the bulk of the plasma which radiates in the L-shell. At 3 ns the T_e estimation includes an added 750 eV contribution which is beyond the L-shell Ni values typically observed on Zebra. With the main implosion fully initiated the hotter plasma is more densely surrounded and the hot electrons can further excite the constrained hot spots. At 8 ns, the estimated highest temperature peaks at 850 eV. The timing of this frame is near the center of the main radiation burst and occurs just before a peak in the 9 keV signal. The next frame maintains the same estimated T_e for the higher and lower temperatures but the middle T_e increases to 480 eV. This occurs during the declining edge of the peak in the 9 keV signal. The last frame recorded the end of the last peak in the 9 keV signal and the beginning of the rapid drop back to zero observed in all the signals except the XRD. The estimated T_e dropped back down to a combination of 450 eV and 100 eV. With the overall decline of the signals this suggests the bulk plasma is beginning to disperse and the hot spots are more readily able to cool down. An example of the individual contributions to the combined spectra used to match the experiment for the 13 ns frame is presented in the last lineout with the 100 eV contribution labeled as I, the 480 eV as II, and the 850 eV as III. Table 2 summarizes the analysis of the K-shell spectra. Both shots are detailed including the frame number for each experiment, the timings relative to the main implosion for each frame, and the electron temperatures of the individual theoretical spectra used to combine into the overall fit.

The spectral features that were modeled and discussed so far are commonly used K-shell satellite lines that were introduced in late 1960s to become a very important part of x-ray plasma spectroscopy diagnostics of both astrophysical and laboratory plasmas [33, 34]. More recently, unusual highly-resolved x-ray spectra were observed using a femtosecond laser-produced plasma that included a new type of satellite

Table 2. Summary of the analysis of three temperature plasma regions (I, II, and III) radiating K-shell x-rays as recorded in shots 3253 and 3254. Individual frames are labeled in the first column along with their relative timings in the second column. All theoretical modeling used a 5×10^{19} cm^{-3} electron density and a 1% hot electron concentration.

		Electron temperature T_e (eV)		
Shot 3253	Timing (ns)	I	II	III
4	−14	100	—	—
5	−9	100	450	—
6	−4	250	450	750
Shot 3254				
2	−2	100	450	—
3	+3	100	450	750
4	+8	100	450	850
5	+13	100	480	850
6	+18	100	450	—

lines identified as being emitted from exotic hollow ion states (for example, KK hollow ions with the empty K shell) [35–39]. Such satellite structures, located between Lyα and Heα resonance lines in low-atomic-number (such as, for example, Al and Si) dense plasmas became very intense when produced by a relativistic laser plasma in the radiation regime [40, 41]. Despite the recent progress in studying these new hollow ion spectroscopic features produced by laser-produced plasmas, there are a very limited number of papers of their observation and identification in Z-pinch plasmas (see [36, 39]). Rosmej *et al* demonstrated that charge exchange of intermixing inhomogeneous plasmas as well as collisions driven by suprathermal (hot) electrons are possible mechanisms to populate hollow ions to observable levels in dense plasmas, particularly in high current Z-pinch plasmas and high intensity field-ionized laser produced plasmas [36, 39]. In addition to considering and modeling K-shell spectra from low-atomic-number hollow ions, such spectra from mid-atomic-number ions (such as, for example, Cu) have been studied [39]. In this paper, we apply our recent studies of the new spectroscopic features radiated from KK hollow ions in low-atomic-number Z-pinch plasmas [42] to the search of such spectroscopic signatures from mid-atomic-number K-shell Ni plasmas.

We calculated atomic data using the FAC for radiative transitions from KK hollow Li-, Be-, B-, C-, N-, and O-like states ($2s^22p^n \rightarrow 1s2s^22p^{n-1}$ for all included states, $2s2p^{n+1} \rightarrow 1s2s2p^n$ for all included states except O-like, $2p^{n+2} \rightarrow 1s2p^{n+1}$ for all included states except N- and O-like) in Ni ions. Altogether, we included 149 levels for Li-like, 312 levels for Be-like, 432 levels for B-like, 492 levels for C-like, 401 levels for N-like, and 269 levels for O-like Ni ions. Theoretical spectra were produced by applying Gaussian broadenings to the radiative decay rate of each transition and combining the resultant profiles. A comparison between theoretical spectra with inclusion of all above-mentioned hollow Ni ions (see figure 4, top) and the experimental spectrum in figure 3(B) recorded at +8 ns after the main x-ray burst (see figure 4, bottom) indicates a good match, for the most intense spectral peaks from Li-, Be-, B-, and C-like Ni ions, and therefore the possible observation of such hollow states in K-shell Ni Z-pinch plasmas.

4. X-ray time-gated L-shell spectroscopy

Soft time-gated L-shell Ni spectra for shot 3253 are presented in figure 5(a). The first two frames do not have any L-shell Ni lines. However, the third frame at 11 ns before the main implosion has the first signs of L-shell Ni radiation. The L-shell presence has a low intensity and limited definition, but it agrees with the fifth frame from the K-shell Ni spectrum in which modeling predicted the hottest regions were comparable to typical L-shell Ni radiation. As the hottest regions would be a smaller portion of the main plasma, the low intensity on the film would make sense. The fourth frame at 6 ns prior to the main implosion shows the first well defined L-shell spectrum. The lineout for this spectrum is included in figure 5(b) along with the theoretical individual ionization contributions of B-like to Na-like Ni ions. Between the various ionizations, most features of the experimental spectrum can be matched. Be-like and Li-like were present in the K-shell but were not included here due to the already cluttered presentation in the case of Be-like and Li-like not having a significant contribution to this spectral region. The two Be-like lines of most significance would be present around 9.75 Å closer to the left B-like line and around 9.63 Å just to the right of the F-like cluster. Ne-like and Na-like were included where they were mostly unexplored in the K-shell due to their clear and resolvable nature in the L-shell radiation.

The lineout from figure 5(b) is compared to non-LTE modeling with an estimated plasma T_e of 350 eV and N_e of 5×10^{19} cm^{-3} in figure 5(c). The modeling matches the experiment very well in the spectral region of 8.75–9.56 Å, the Ne-like 4 C ($1s^22s^22p_{1/2}2p^4{}_{3/2}4d_{3/2}$ $J = 1 \rightarrow 1s^22s^22p^6$ $J = 0$) and 4D ($1s^22s^22p^2{}_{1/2}2p^3{}_{3/2}4d_{5/2}$ $J = 1 \rightarrow 1s^22s^22p^6$ $J = 0$) lines, and the spectral structure in the 10.67–11.08 Å region. The region beyond 11.08 Å is overestimated and this

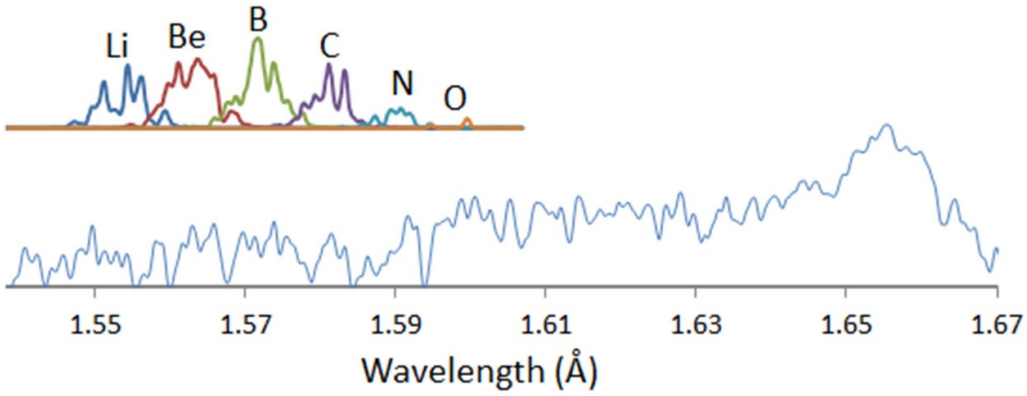

Figure 4. (Top) Theoretical spectrum produced from hollow ion transitions separated by ionic state. (Bottom) experimental spectrum from figure 3(B) representing the radiation at +8.

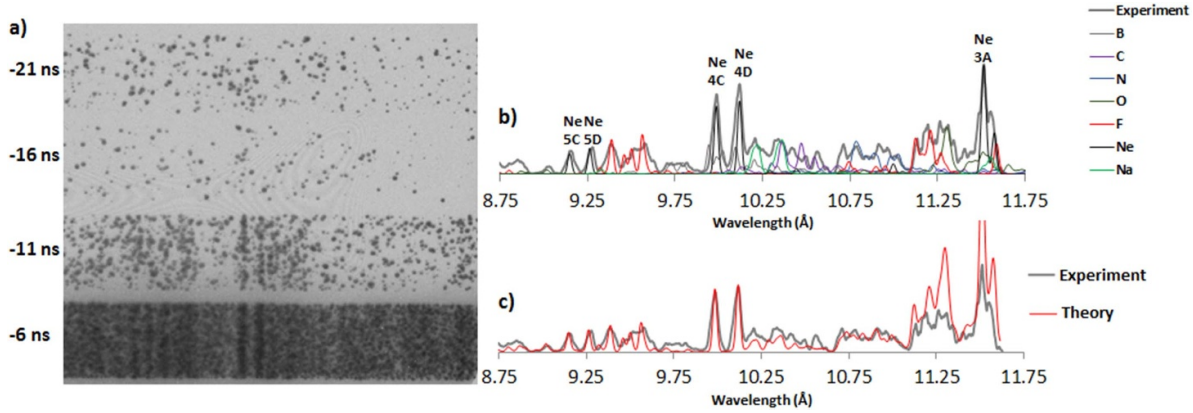

Figure 5. Zebra shot 3253. (a) Film from the TGSP spectrometer with early timings relative to the main x-ray burst. (b) Lineout of L-shell Ni spectrum from the last frame (−6 ns) with theoretical spectra from individual ionizations shown for reference. (c) Lineout of the L-shell Ni spectrum from the last frame (−6 ns) of the TGSP spectrometer compared to non-LTE kinetic modeling at estimated plasma conditions of $T_e = 350$ eV and $N_e = 5 \times 10^{19}$ cm^{-3}.

is due to the modeling not including any corrections for opacity effects. These lines are primarily from Ne-like and F-like $n = 3 \rightarrow 2$ transitions which are the most heavily populated levels for the estimated plasma conditions and are therefore the most affected by opacity. The Ne-like 4C, 4D, 5C ($1s^2 2s^2 2p_{1/2} 2p^4{}_{3/2} 5d_{3/2}$ $J = 1 \rightarrow 1s^2 2s^2 2p^6$ $J = 0$), and 5D ($1s^2 2s^2 2p^2{}_{1/2} 2p^3{}_{3/2} 5d_{5/2}$ $J = 1 \rightarrow 1s^2 2s^2 2p^6$ $J = 0$) lines and the F-like lines between them are from higher Rydberg states which lead to lower populations and therefore are less affected by opacity. Lines that have low opacity effects require fewer assumptions to properly fit and therefore increase confidence in the modeling when matched. For these reasons, matching the higher Rydberg states with the theoretical modeling is the primary goal. The two regions that are more noticeably underestimated by the modeling are the spectral features surrounding 9.75 Å and to the right of the Ne-like 4D line. The spectral features around 9.75 Å along with the nearby edge to the left are lines produced from B-like and Be-like Ni. The structure to the right of the Ne 4D line is primarily composed of Na-like, C-like, and B-like Ni transitions. With the current plasma condition estimation Na-like Ni makes up around 7% of the total composition and C-, B-, and Be-like Ni are not significantly populated. The underestimating by the theory can be attributed to the presence of a smaller fraction of hotter plasma, as observed in the K-shell spectra. Increasing the presence of the higher ionizations (C-, B-, and Be-like) can be achieved by increasing the estimated T_e. As the T_e is increased, the ionization balance will shift to increase the percentage of F-, O-, and N-like Ni faster than the higher ionizations which would result in a poorer match overall and is the reason why this particular modeling was chosen.

The L-shell spectrometer for shot 3254 recorded data at times comparable to the middle four frames of the K-shell spectrometer. The film is shown in figure 6 along with lineouts and modeling for comparison. The estimated plasma conditions were slightly variable with T_e between 350 and 370 eV and N_e of 5×10^{19} cm^{-3}. Similar to what was described for shot 3253, the main differences between the theory and experiment lie in the locations of higher ionization stages and the overestimated optically thick regions. The first frame shows a similar difference as was seen in shot 3253. In the following frame, the theory fits closer and this is likely due to the greater bulk plasma presence as the main implosion progresses. This leads to the hot spots being overshadowed and therefore a weaker presence in the observed spectra. The third frame has the greatest disagreement with the theory. This frame aligns

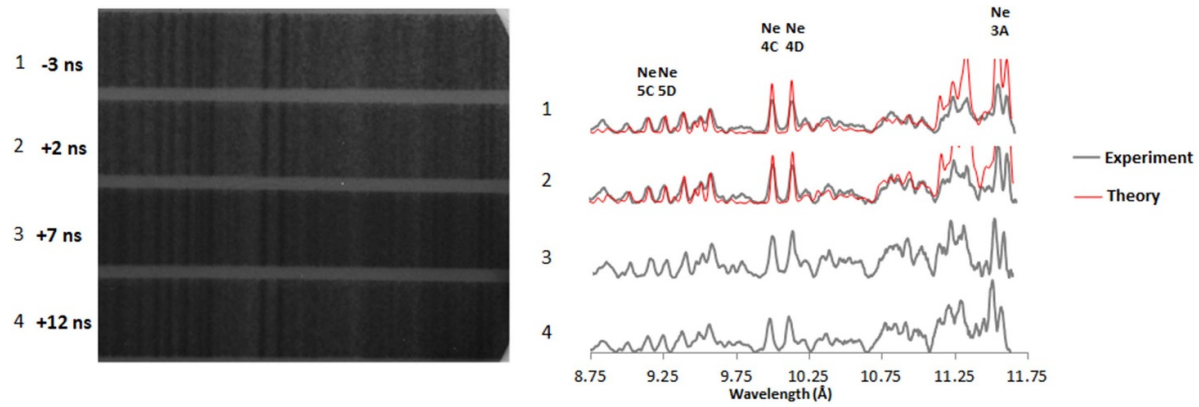

Figure 6. Zebra shot 3254. (a) Film from the TGSP spectrometer with later timings relative to the main x-ray burst. (b) Lineouts of the L-shell Ni spectra recorded by the TGSP spectrometer compared to non-LTE kinetic modeling at estimated plasma conditions of $N_e = 5 \times 10^{19}$ cm^{-3} and T_e varied slightly between 350 eV (-3 ns) and 370 eV ($+2$ ns, $+7$ ns, and $+12$ ns).

with the maximum temperature observed in the K-shell. As the L-shell plasma conditions remain consistent, the higher hot spot temperature suggests a greater intensity of radiation from the high ionizations which lead to a greater presence in the L-shell. The last frame coincides with the first dip in the T_e from the K-shell and a closer match to the theory is found in the L-shell.

5. Conclusion

Alumel DPWA Z-pinch experiments were performed on the Zebra generator at the enhanced current of 1.6 MA with an advanced setup of diagnostics to measure the temporal evolution of x-ray radiation from plasmas. The two experiments varied only in the total mass (192 μg and 173 μg) with the major focus on simultaneously recording time-gated K-shell and L-shell Ni spectra and comparison with the corresponding x-ray diode signals. Between the two experiments, a wide observation window was established around the main x-ray burst. The TGHXR spectrometer was able to record hard x-ray K-shell Ni radiation between -14 ns and $+18$ ns while the TGSP spectrometer was able to record soft x-ray L-shell Ni radiation during similar times, between -11 ns and $+12$ ns counted from the main implosion.

All time-gated hard x-ray K-shell Ni spectra display the 'cold' Kα Ni line as the most intense line in their spectra. Starting at -14 ns, the first Kα Ni lines were observed, which were identified as primarily Ne-like Ni and lower ionization stages with a maximum ionization stage of O-like Ni. The observed ionization stages proceeded to expand to peak with Li-like Ni at -4 ns for shot 3253 and 8 ns for shot 3254. Finally the ionization stages began to reduce back down to a peak of C-like Ni at the last recorded frame of 18 ns. Combined theoretical spectra from up to three different electron temperatures plasma regions were fitted to the experimental spectra with electron densities of 5×10^{19} cm^{-3} and hot electron percentages of 1%. The corresponding three electron temperatures varied from low values between 100 and 250 eV (I), to moderate values between 450 or 480 eV (II), up to the high values between 750 and 850 eV (III). Having three different plasma regions evidences the non-uniform Z-pinch plasmas.

Along with estimations of the K-shell plasma ionization balance and conditions, spectral features in the 1.55–1.59 Å spectral range were compared to theoretical spectra produced using atomic data from exotic hollow ion states. The hollow ion spectra were separated into ionization stages from Li-like to O-like Ni and provided a good match to the experimental spectrum at the highest value of $T_e = 850$ eV. This provides additional support for the presence of such exotic ion states in Z-pinch plasmas for which there has been very little information previously outside laser produced plasmas.

Starting at -11 ns with the first signs of L-shell Ni radiation, pronounced L-shell radiation of almost the same intensity was present for the remaining observation period which ended with the last recorded frame at $+12$ ns. Non-LTE modeling of the L-shell Ni spectra found a consistent electron temperature with only small variation between 350 and 370 eV. It appears that including hot electrons was not necessary to improve the modeling of the L-shell Ni.

By considering both K-shell and L-shell time-gated radiation of Ni ions, more conclusions can be drawn. Overall, time-gated plasma spectroscopy definitely provides more information on temporal evolution of 'hot' and 'cold' K-shell plasmas though some of the L-shell spectral features manifest the temporal changes as well. For example, while the L-shell radiation was dominated by near Ne-like Ni, there were two spectral regions where Be-, B-, and C-like Ni were observed that exceeded the predictions of the theoretical estimations. These regions varied in relative intensity compared to the estimations, with the greatest variations coinciding with the greatest degree of ionization observed in the K-shell. Comparing the estimated parameters shows the maximum electron temperatures observed in the K-shell Ni plasma always exceeded the estimations from the L-shell Ni plasma.

This confirms the presence of bright spots with hot electrons in K-shell plasma that in general evolves much faster in time than bulk L-shell plasma. In addition, the new spectral features such as from hollow ions can be observed and studied using the time-gated K-shell plasma spectroscopy, which is important for further investigation of exotic ion states in plasmas.

Data availability statement

All data that support the findings of this study are included within the article (and any supplementary files).

Funding

This research was supported by National Nuclear Security Administration (NNSA) under DOE Grant DE-NA0004133 and by the National Science Foundation and the NNSA under NSF award PHY-2205769.

ORCID iDs

A Stafford https://orcid.org/0009-0008-4147-6052
A S Safronova https://orcid.org/0000-0001-6160-4009

References

[1] Haines M G 2011 *Plasma Phys. Control. Fusion* **53** 093001
[2] Matzen M K *et al* 2005 *Phys. Plasmas* **12** 55503
[3] Pereira N R 2020 *Matter Radiat. Extremes* **5** 026402
[4] Cuneo M E *et al* 2006 *Phys. Plasmas* **13** 056318
[5] Ampleford D J *et al* 2010 *Phys. Plasmas* **17** 056315
[6] Lebedev S V, Frank A and Ryutov D D 2019 *Rev. Mod. Phys.* **91** 2
[7] Lebedev S V *et al* 2005 *Plasma Phys. Control. Fusion* **47** B465
[8] Yager-Elorriaga D A *et al* 2022 *Sinars Nucl. Fusion* **62** 042015
[9] Shrestha I, Kantsyrev V L, Safronova A S, Esaulov A A, Williamson K M, Ouart N D, Osborne G C, Weller M E and Yilmaz M F 2010 *IEEE Trans. Plasma Sci.* **34** 658–66
[10] Childers R R, Safronova A S, Kantsyrev V L, Stafford A and Gill A K 2023 *J. Quant. Spectrosc. Radiat. Transfer* **303** 108586
[11] Safronova A S, Kantsyrev V L, Weller M E, Shlyaptseva V V, Shrestha I K, Stafford A, Schmidt-Petersen M T, Lorance M Y, Schultz K A and Chuvatin A S 2016 *Phys. Plasmas* **23** 101210
[12] Safronova A S, Esaulov A A, Kantsyrev V L, Ouart N D, Shlyaptseva V, Weller M E, Keim S F, Williamson K M, Shrestha I and Osborne G C 2011 *High Energy Density Phys.* **7** 252
[13] Kantsyrev V L *et al* 2014 *Phys. Plasmas* **21** 031204
[14] Coverdale C A *et al* 2010 *High Energy Density Phys.* **6** 143
[15] Stafford A, Safronova A S, Kantsyrev V L, Keim S F, Weller M E, Shrestha I and Shlyaptseva V V 2016 *Phys. Plasmas* **23** 101209
[16] Whitney K G, Thornhill J W, Apruzese J P and Davis J 1990 *J. Appl. Phys.* **67** 1725
[17] Thornhill J W *et al* 2006 *IEEE Trans. Plasma Sci.* **34** 2377
[18] Safronova A S *et al* 2012 *IEEE Trans. Plasma Sci. Z-Pinch Plasmas* **40** 3347–52
[19] Beiersdorfer P, May M J, Scofield J H and Hansen S B 2012 *High Energy Density Phys.* **8** 271
[20] Lee R W, Nash K and Ralchenko Y 1997 *J. Quant. Spectrosc. Radiat. Transfer* **58** 737
[21] Bowen C, Decoster A, Fontes C J, Fournier K B, Peyrusse O and Ralchenko Y V 2003 *J. Quant. Spectrosc. Radiat. Transfer* **81** 71
[22] Rubiano J G, Florido R, Bowen C, Lee R W and Ralchenko Y 2007 *High Energy Density Phys.* **3** 225
[23] Fontes C J, Abdallah J Jr, Bowen C, Lee R W and Ralchenko Y 2009 *High Energy Density Phys.* **5** 15
[24] Ouart N D *et al* 2011 *J. Phys.* B **44** 065602
[25] Bauer B S, Kantsyrev V L, Winterberg F, Shlyaptseva A S, Mancini R C, Li H and Oxner A 1997 *AIP Conf. Proc.* **409** 153–6
[26] Chuvatin A S *et al* 2010 *Phys. Rev. Spec. Top. Accel. Beams* **13** 010401
[27] Esaulov A A, Kantsyrev V L, Safronova A S, Velikovich A L, Shrestha I K, Williamson K M and Osborne G C 2012 *Phys. Rev. E* **86** 046404
[28] Williamson K M, Kantsyrev V L, Esaulov A A, Safronova A S, Cox P, Shrestha I, Osborne G C, Weller M E, Ouart N D and Shlyaptseva V V 2010 *Phys. Plasmas* **17** 112705
[29] Gu M F 2008 *Can. J. Phys.* **86** 675–89
[30] Hansen S 2003 Development and application of L-shell spectroscopic modeling for plasma diagnostics *PhD Dissertation* University of Nevada, Reno
[31] Ouart N D, Safronova A S, Kantsyrev V L, Esaulov A A, Williamson K M, Shrestha I, Osborne G C and Weller M E 2010 *IEEE Trans. Plasma Sci.* **34** 631–8
[32] Ouart N D 2010 Radiative properties of Z-pinch and laser produced plasmas from mid-atomic-number materials *PhD Dissertation* University of Nevada, Reno
[33] Gabriel A H and Jordan C 1969 *Nature* **221** 947–9
[34] Gabriel A H 1972 *Mon. Notice R. Astron. Soc.* **160** 99–119
[35] Faenov A Y *et al* 1999 *Phys. Scr.* **T80** 536
[36] Rosmej F *et al* 2001 *Nucl. Instrm. Methods Phys. Res.* A **464** 257
[37] Faenov A Y *et al* 2011 *JETP Lett.* **94** 171
[38] Safronova A S *et al* 2012 *High Energy Density Phys.* **8** 190
[39] Rosmej F B, Dachicourt R, Deschaud B, Khaghani D, Dozières M, Šmíd M and Renner O 2015 *J. Phys.* B **48** 224005
[40] Colgan J *et al* 2013 *Phys. Rev. Lett.* **110** 125001
[41] Colgan J *et al* 2016 *Europhys. Lett.* **114** 35001
[42] Safronova A S, Kantsyrev V L, Prins N S, Panter K, Childers R R and Shlyaptseva V V 2023 New spectroscopic features radiated from low-atomic-number Z-pinch plasmas *2023 IEEE Int. Conf. on Plasma Science (ICOPS)* pp 1